Microstructural Analysis of Interface Modification by Silane Coupling Agents in Asphalt-Grout ITZ of Semiflexible Pavements

Liu, Xiaoyu; Wu, Kuanghuai; Li, Yi; Giacomello, Giovanni; Yue, Yunpeng; Ren, Fengming; Pasetto, Marco

DOI
10.1061/JMCEE7.MTENG-20997

Publication date
2025

Document Version
Final published version

Published in
Journal of Materials in Civil Engineering

Citation (APA)
Liu, X., Wu, K., Li, Y., Giacomello, G., Yue, Y., Ren, F., & Pasetto, M. (2025). Microstructural Analysis of Interface Modification by Silane Coupling Agents in Asphalt-Grout ITZ of Semiflexible Pavements. *Journal of Materials in Civil Engineering*, *38*(1), Article 04025479. https://doi.org/10.1061/JMCEE7.MTENG-20997

Microstructural Analysis of Interface Modification by Silane Coupling Agents in Asphalt–Grout ITZ of Semiflexible Pavements

Xiaoyu Liu, Ph.D.[1]; Kuanghuai Wu, Ph.D.[2]; Yi Li, Ph.D.[3]; Giovanni Giacomello, Ph.D.[4]; Yunpeng Yue, Ph.D.[5]; Fengming Ren, Ph.D.[6]; and Marco Pasetto, Ph.D.[7]

Abstract: Semiflexible pavement (SFP) is a composite material composed of porous asphalt mixtures and cementitious grout substances. Numerous asphalt–grout interfacial transition zones (ITZ) exist within this material and present inherent susceptibility to cracking. However, the microstructural changes within these interfaces remain inadequately understood due to the material's complex and multiphase nature. This study investigates the microstructural characteristics of the asphalt–grout ITZ and its relationship with SFP's macroscale performance, focusing on silane coupling agent modification. Atomic force microscopy (AFM) was first employed to analyze the effects of curing age, grout strength, and interfacial modification. Then, scanning electron microscopy (SEM) analysis was used to explore the correlation between the micromorphology and macroscopic mechanical properties of the asphalt–grout ITZ. Finally, a semicircular bending test was applied to test the crack resistance of SFP after interface modification. The results show that immersion of the porous asphalt mixture specimens with the interface modifier can enhance the microscopic properties of the asphalt and cementitious grout materials. The ITZ between asphalt and grout forms a double-layer structure, with smoother interfaces observed after applying the interfacial modifier. The width of the asphalt–grout ITZ may exceed 30 μm after SFP formed for 28 days. Microcracks in the asphalt–grout ITZ were significantly reduced after interface modification. These findings provide insights into proactive strategies for reducing cracking at asphalt–grout interfaces, thereby enhancing the overall performance of SFP. **DOI: 10.1061/JMCEE7.MTENG-20997.**

Author keywords: Semiflexible pavement (SFP); Asphalt–grout interfacial transition zone (ITZ); Interfacial modifier; Atomic force microscopy (AFM); Silane coupling agent.

Introduction

Semiflexible pavement (SFP) material is a unique type of road material composed of a porous asphalt mixture (PAM) and cementitious grout material, with the void content of the asphalt mixture typically ranging from 20% to 35% (Pei et al. 2016; Sui et al. 2024). Compared to traditional asphalt mixtures, SFP offers improved rutting resistance, as well as higher compressive and shear strength (Zhao and Yang 2022). These characteristics make SFP particularly effective in addressing common issues in asphalt pavements, such as rutting and water damage. It shows promise for use in heavy-load pavements, intersections, bus stops, and other specialized areas (Hu et al. 2023).

In SFP, two main interfacial transition zones (ITZs) (Cheng et al. 2023; Liu et al. 2025a) exist: the aggregate-asphalt interface and the asphalt–grout interface, with the latter being the primary interface and often regarded as the weakest point in SFP materials (Cheng et al. 2023; Wang et al. 2021). The ITZ between asphalt and cementitious grout plays a significant role, as cracking at these interfaces is one of the main failure modes of SFP (Liu et al. 2025b; Zhang et al. 2024b). Consequently, in addition to the complex construction techniques and high costs, cracking represents a primary barrier to the promotion of SFP (Wu et al. 2021). Previous studies (Cai et al. 2020a; Ling et al. 2022a) have demonstrated that the application of interfacial modifiers, such as silane coupling agents, can enhance the crack resistance of SFP (Davoodi et al. 2022; Fan et al. 2024; Lin et al. 2022). Liu et al. (2023) research indicated that SFP constructed with low-strength grout material can improve asphalt–grout interfacial adhesion through the application of a silane coupling agent solution, leading to enhanced mechanical properties across the entire SFP. While these improvements have primarily been observed at the macroscopic level, the underlying microstructural mechanisms that drive these enhancements remain poorly understood. Characterizing the internal structural changes within SFP is crucial for elucidating the mechanisms of microstructural damage and their effects on overall performance (Cai et al. 2019). The macroscopic behavior of SFP is closely tied to changes in the microscopic mechanical properties at the composite interface

[1]Postdoctoral Researcher, School of Civil Engineering and Transportation, Guangzhou Univ., 230 Waihuanxi Rd., Daxuecheng, Guangzhou 361005, China. ORCID: https://orcid.org/0000-0003-4343-1591. Email: xiaoyuliu@gzhu.edu.cn

[2]Professor, School of Civil Engineering and Transportation, Guangzhou Univ., 230 Waihuanxi Rd., Daxuecheng, Guangzhou 361005, China (corresponding author). Email: wukuanghuai@163.com.

[3]Assistant Professor, Section of Pavement Engineering, Faculty of Civil Engineering and Geosciences, Delft Univ. of Technology, Stevinweg 1, Delft 2628 CN, Netherlands. ORCID: https://orcid.org/0000-0002-6799-7007. Email: Y.Li-41@tudelft.nl

[4]Assistant Professor, Dept. of Civil, Environmental, and Architectural Engineering, Univ. of Padova, via Marzolo 9, Padova 35131, Italy. ORCID: https://orcid.org/0000-0003-1436-1475. Email: giovanni.giacomello@unipd.it

[5]Postdoctoral Researcher, School of Civil Engineering and Transportation, Guangzhou Univ., 230 Waihuanxi Rd., Daxuecheng, Guangzhou 361005, China. Email: yueyunpeng@gzhu.edu.cn

[6]Professor, School of Civil Engineering and Transportation, Guangzhou Univ., 230 Waihuanxi Rd., Daxuecheng, Guangzhou 361005, China. Email: rfm@gzhu.edu.cn.

[7]Professor, Dept. of Civil, Environmental and Architectural Engineering, Univ. of Padova, via Marzolo 9, Padova 35131, Italy. Email: marco.pasetto@unipd.it

Note. This manuscript was submitted on November 28, 2024; approved on March 26, 2025; published online on October 21, 2025. Discussion period open until March 21, 2026; separate discussions must be submitted for individual papers. This paper is part of the ***Journal of Materials in Civil Engineering***, © ASCE, ISSN 0899-1561.

(Lai et al. 2024). Traditional laboratory tests that measure macroscopic parameters often fail to capture the complexities of microstructural damage in SFP materials (Zhang et al. 2023a). Therefore, a microscale analysis is essential for clarifying the load transfer mechanisms involved (Gao et al. 2023; Qiang et al. 2011). To investigate the adhesion properties at the asphalt–grout interface, researchers have begun employing microscopic techniques, including fluorescence microscopy (Abdessalem et al. 2021; Xie et al. 2023; Zhang et al. 2024c) and scanning electron microscopy (SEM) (Hoy et al. 2018; Pouliot et al. 2003). Zhu et al. (2017) employed nanoscale metrology to examine the micromechanics, microstructure, and chemistry of ITZ in mastic and aggregate surfaces. Their results identified ITZ as a weak link in asphalt mixtures, with a thickness of 5–20 μm and a modulus between that of the aggregate and mastic. Zhao et al. (2023) investigated the effects of thermal aging and moisture on the micromechanical properties of ITZ in PA mixtures. The results found that ITZ thickness ranges from 10–20 μm, with aging increasing the modulus of both asphalt mastic and ITZ, while moisture reduces ITZ modulus and slightly increases its width. Thermal aging had little impact on ITZ thickness. ITZ is typically 10–50 μm thick in concrete and asphalt mixtures and plays a crucial role in mechanical behavior, durability, and resistance to external factors (Xu et al. 2022). Its molecular and atomic characteristics govern interactions between asphalt mastic and aggregate and influence adhesion, cohesion, and load transfer efficiency (Xu et al. 2020). Chemical bonding, van der Waals forces, and polar interactions determine the strength of asphalt-aggregate adhesion and directly affect ITZ performance (Guo et al. 2020). However, existing research methods have not adequately revealed the effects of interface properties at the molecular and atomic levels, nor have they explored how nanoscale interactions at the asphalt–grout interface influence the macroscopic properties of SFP (Cui et al. 2021).

Despite the known benefits of interfacial modification, most existing studies have concentrated on the macroscopic modifications of grout materials (Raza and Sharma 2024) and the mixing proportions of matrix mixtures (Zarei et al. 2022; Zhang et al. 2024a), with limited research addressing the factors influencing properties, such as the microscopic evolution of the asphalt–grout ITZ (Cai et al. 2021). The microstructural evolution of SFP before and after such reinforcement has not been thoroughly examined, and this gap in knowledge hinders a deeper understanding of the mechanisms that influence overall pavement performance. Therefore, further investigation is necessary to clarify the damage process occurring at the ITZ and its influence on SFP performance using micromechanics techniques (Ling et al. 2021, 2022b). This paper investigates the microstructural interface properties of SFP with varying strengths of grout materials, both before and after interface reinforcement using micromechanics techniques. The ITZ between asphalt and grout of SFP was tested using atomic force microscopy (AFM) (Allen et al. 2012) with different grout strengths, different curing ages, and interface modifications. Additionally, the impacts of the ITZ between asphalt and grout before and after applying interface modifiers are analyzed using SEM. The results can be used to characterize the mechanical properties of SFP composites under the composite interface microstructure.

Therefore, this study aims to bridge the gap by investigating the microstructural characteristics of the asphalt–grout interface in SFP, particularly after immersion in a silane coupling agent solution. By linking these microstructural insights to macroscopic performance, this research seeks to provide strategies for improving the durability and resilience of SFP in road construction.

Materials and Methods

Materials

Asphalt and Aggregate

A representative styrene-butadiene-styrene block copolymers (SBS)-modified asphalt sample was selected for this study. Table 1 lists the parameters of the SBS-modified asphalt. The coarse aggregates were natural diabase. The SBS content is 4.1% by weight, and the specifications of rheological properties of the applied SBS-modified asphalt are depicted in Table 2.

SFP consists of an open-graded asphalt mixture skeleton and cement grouting material. The gradation design is listed in Fig. 1. The asphalt content is 4.5% by weight. The particle size distribution of the PAM specimens is as follows: aggregates with a size range of 9.5–13.6 mm account for 63.1%, while those in the ranges of 4.75–9.5 mm and 2.36–4.75 mm constitute 24.9% and 8.5%, respectively. Mineral powder comprises 3.5% of the mixture, and the bitumen-to-aggregate ratio is 3.6%. The void ratio of the PAM specimens was determined using the volume method, as specified

Table 1. Specifications of the asphalt

Properties	Technical requirements	Test results
Elastic recovery ratio @25°C (%)	≥90	95.0
Ductility @5°C and 5 cm/min (cm)	>20	32.0
Penetration @25°C,100 g, and 5 s (0.1 mm)	40–60	54
Penetration index (PI)	≥0	0.06
Storage stability (softening point)@163°C and 48 h (°C)	≤2.5	1
Softening point R&B (°C)	>70	88.5
Viscosity @135°C (pa · s)	≤3.0	2.36

Note: The asphalt was produced by Shell Xinyue (Foshan) Asphalt.

Table 2. Rheological properties of the applied SBS-modified asphalt

Properties	Unit	Test results
Performance grade (PG)	—	76–22
Complex shear modulus @64°C (G*)	kPa	16.35
Phase angle @64°C (δ)	Degrees	67
Creep stiffness @-12°C (S)	MPa	95.20
m-value @-12°C	—	0.50

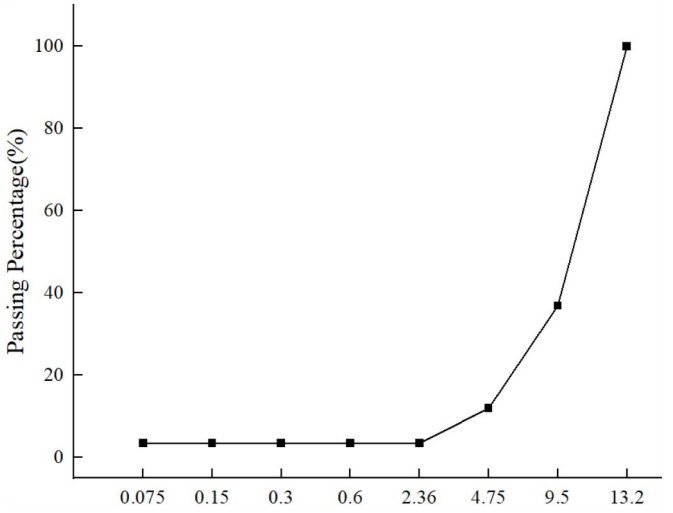

Fig. 1. Gradations of the aggregates.

Table 3. Specifications of the grout materials

Materials	Water–binder ratio	Compressive strength (28 days) (MPa)	Flexural strength (28 days) (MPa)	Tensile strength (MPa)	Fluidity (s)
GM-40	0.32	36.88	8.30	1.11	10
GM-60	0.30	57.02	10.30	2.02	16
GM-70	0.27	70.00	11.90	1.19	11

Note: GM-40, GM-60, and GM-70 denote grout material named Sobute, Sino, and Unikrete respectively produced by Sobute New Materials Co., Ltd., Beijing Sino-Sina Building Technolgy Co., Ltd., and Zhejiang Weihua New Building Materials Co., Ltd.

in Chinese standard JT/T E20-2017 (Chinese Standard 2011), and ranged from 28% to 30%.

Grout Materials

Three types of grout materials, each with varying strengths, were utilized. The specifications of the grout materials are depicted in Table 3. The water–binder ratios for these materials were provided as recommendations by the manufacturers.

Interfacial Modifier

Previous work (Liu et al. 2023) has demonstrated that the mechanical properties of the composite interface in SFP materials can be enhanced by grouting the PAM specimens after immersion them with a silane coupling agent solution. In this study, the silane coupling agent KH-570, a colorless clear liquid with a chromatographic purity of ≥98%, a density of 1.02–1.06 g/cm^3, and a refractive index of 1.426–1.435 at 25°C, was employed to enhance the properties of the asphalt–grout interface. A solution of 72% methanol, 20% silane coupling agent, and 8% water was prepared for immersion in the samples. Fig. 2 illustrates the experimental steps of the interface immersion using a silane coupling agent. Standard-sized PAM specimens were molded according to specifications, the PAM specimens were cooled to room temperature, and the grout material was poured into them. During the grouting process, the specimens are vibrated for 1–3 min using a small shaker to promote grouting. In order to explore the effects of the asphalt–grout interfacial strength on the overall mechanical properties of the SFP, the as-formed PAM specimens were immersed in the silane coupling agent solution for 1 h and then grouted to obtain SFP specimens.

Atomic Force Microscope Test

AFM Sample Preparation

The AFM test was conducted to analyze the interface properties of three types of grout materials with varying strengths at different curing ages, i.e., 3 days, 7 days, 14 days, and 28 days. The instrument mode used was a Dimension ICON AFM (Bruker, Germany). The probe used was type P/N MPP-11120-10, made of silicon (Fan et al. 2021). The cantilever has a nominal elastic modulus of 40 N/m, a tip height of 10–15 μm, and a tip radius of curvature of 8 nm. The scanning resolution used in this experiment is 256 × 256, and the scanning frequency is 0.5 Hz.

Since polishing will cause the resin material that encapsulates the asphalt to mix into the asphalt, affecting the observation results of asphalt–grout ITZ during AFM testing. Therefore, a special method was used instead of polishing in this study. The asphalt–grout interface sample of SFP samples was prepared on glass slides, and asphalt was heated in an oven until it became flowable. Then, a suitable amount was dropped onto the slide. After cooling, premixed cementitious grout materials were poured to fully encase the asphalt, as depicted in Fig. 3. AFM grouting is to drip the grout around the asphalt to form asphalt–grout naturally. Epoxy resin two-component adhesive glue was used to attach another slide on top. Then, the sample was placed in a −15°C refrigerator for 2 h to freeze. After freezing, the first slide was removed, leaving a flat surface. The surface roughness of the sample could be kept below 5 μm during preparation. The asphalt film thickness in asphalt mixture typically ranges from 5 to 20 μm (Kandhal and Chakraborty 1996). In this study, the oil-stone ratio is 4.7, resulting in an asphalt

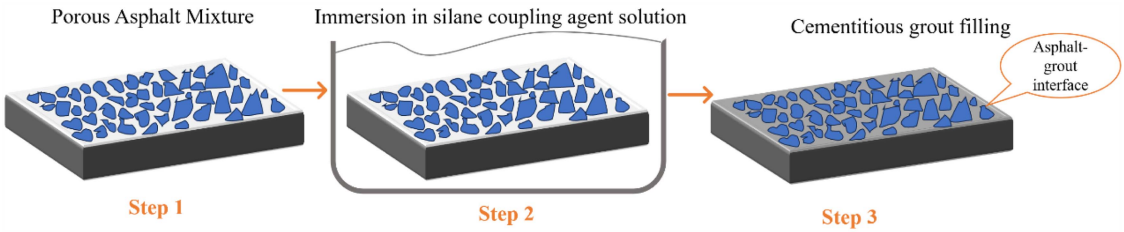

Fig. 2. Flowchart of SFP specimens with a silane coupling agent solution.

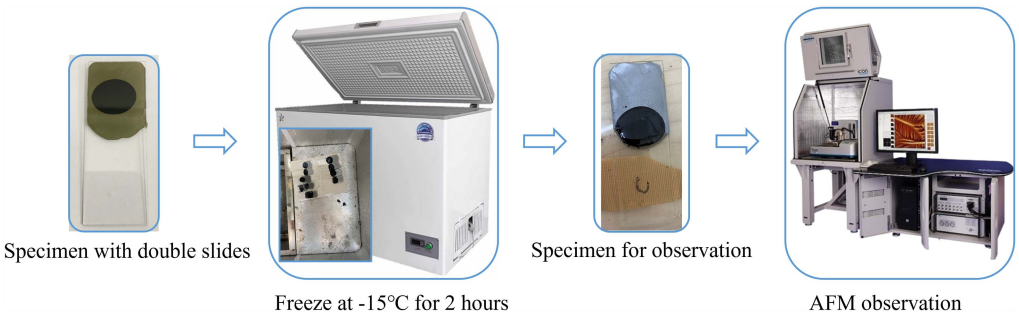

Fig. 3. The pre-process and the sample result for the AFM test. (Images by author Xiaoyu Liu.)

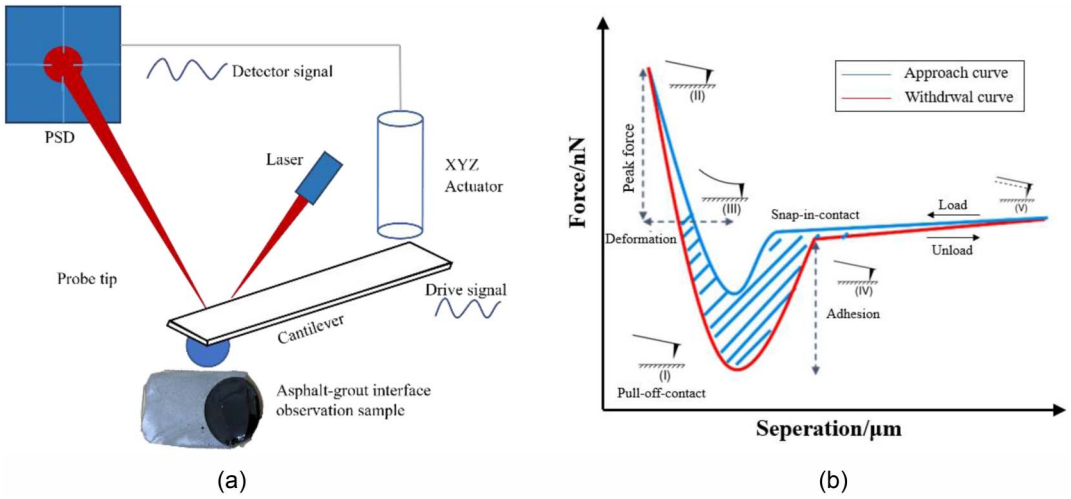

Fig. 4. Principle of (a) PF-QNM mode using AFM and (b) the force-displacement curve.

film thickness of 10.8 μm. The AFM measurement area is 15 μm wide, ensuring that the observed region fully encompasses the asphalt film. Therefore, the asphalt film width measured by AFM aligns with actual engineering conditions.

PF-QNM Mode

The peak force quantitative nanomechanical mapping (PF-QNM) mode is used to analyze the AFM results (Gao et al. 2019). Four metrics, including height, DMT modulus, adhesion, and dissipation, have been used to evaluate the interface properties of SFP materials. This method is composed of two steps, peak force tapping (PFT) mode for imaging, and QNM for characterization (Ren et al. 2019).

The principle of PF-QNM mode in the AFM test is shown in Fig. 4. The probe comprises a tip and a cantilever and is utilized to examine the sample surface using a sinusoidal wave probe. As the force reaches the predetermined peak force, it serves as a feedback signal, providing physical and mechanical insights into the interaction between the tip and the sample at each point. This process includes two stages, i.e., forward and backward. During the backward process of the tip, the van der Waals force generates a peak attraction, denoted as the adhesion force F_{adh} between the tip and the SFP sample. The area enclosed by the peak force vs tip separation distance curve represents the dissipated energy. The elastic modulus of the material E^* can be calculated by

$$F_{tip} = \frac{4}{3}E^*\sqrt{R(d-d_0)^3} + F_{adh} \tag{1}$$

$$E^* = \left[\frac{1-v_s^2}{E_s} + \frac{1-v_{tip}^2}{E_{tip}}\right]^{-1} \tag{2}$$

where F_{tip} = peak force of the tip; R = radius of curvature of the tip; d = radius of the scanning tube; d_0 = cantilever deformation; v_s and v_{tip} = Poisson's ratios of the pattern and the tip, respectively; E_s and E_{tip} = elastic moduli of the pattern and the tip respectively.

Scanning Electron Microscopy Test

Besides the AFM test, the SEM test was conducted to examine the microscopic morphology of the ITZ between asphalt and grout in SFP materials after interface modification, as shown in Fig. 5. To facilitate this analysis, the surface of the SFP sample was sectioned

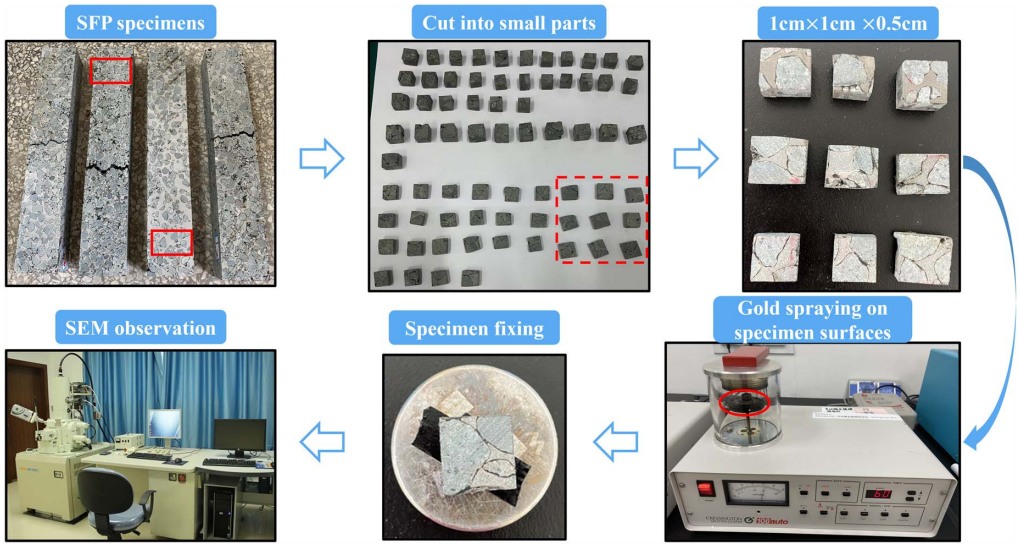

Fig. 5. The main step of the SEM test. (Images by author Xiaoyu Liu.)

J. Mater. Civ. Eng., 2026, 38(1): 04025479

to prepare a batch of small specimens of the ITZ, each measuring 1 cm × 1 cm × 0.5 cm.

Semicircular Bending Test

To test the crack resistance of SFP after interface modification, the semicircular bending test was applied according to the standard of AASHTO-TP-124-16 (AASHTO 2016). The hardening models were compacted into cylindrical specimens with a diameter of 150 mm and a height of 170 mm using GM-40 grouting material. Subsequently, each specimen was halved to obtain semicircular bending test specimens. The semicircular bending test specimens were prepared by cutting the cylindrical samples, resulting in a diameter of 150 mm and a thickness of 50 mm. A centrally located notch, 15 mm in length, was introduced at the bottom of each specimen. The experiments were conducted at a temperature of 25°C with a loading rate of 2 mm/min.

Results

Curing Ages Analysis

Fig. 6 shows the microstructural characteristics of the asphalt–grout interface in SFP materials with different curing ages using the AFM method. Note that only the GM-60 grout materials are shown, as this strength is widely used in SFP. The results in Fig. 6(a) show that with increasing curing age, the interaction boundary of the asphalt–grout composite interface becomes more and more blurred.

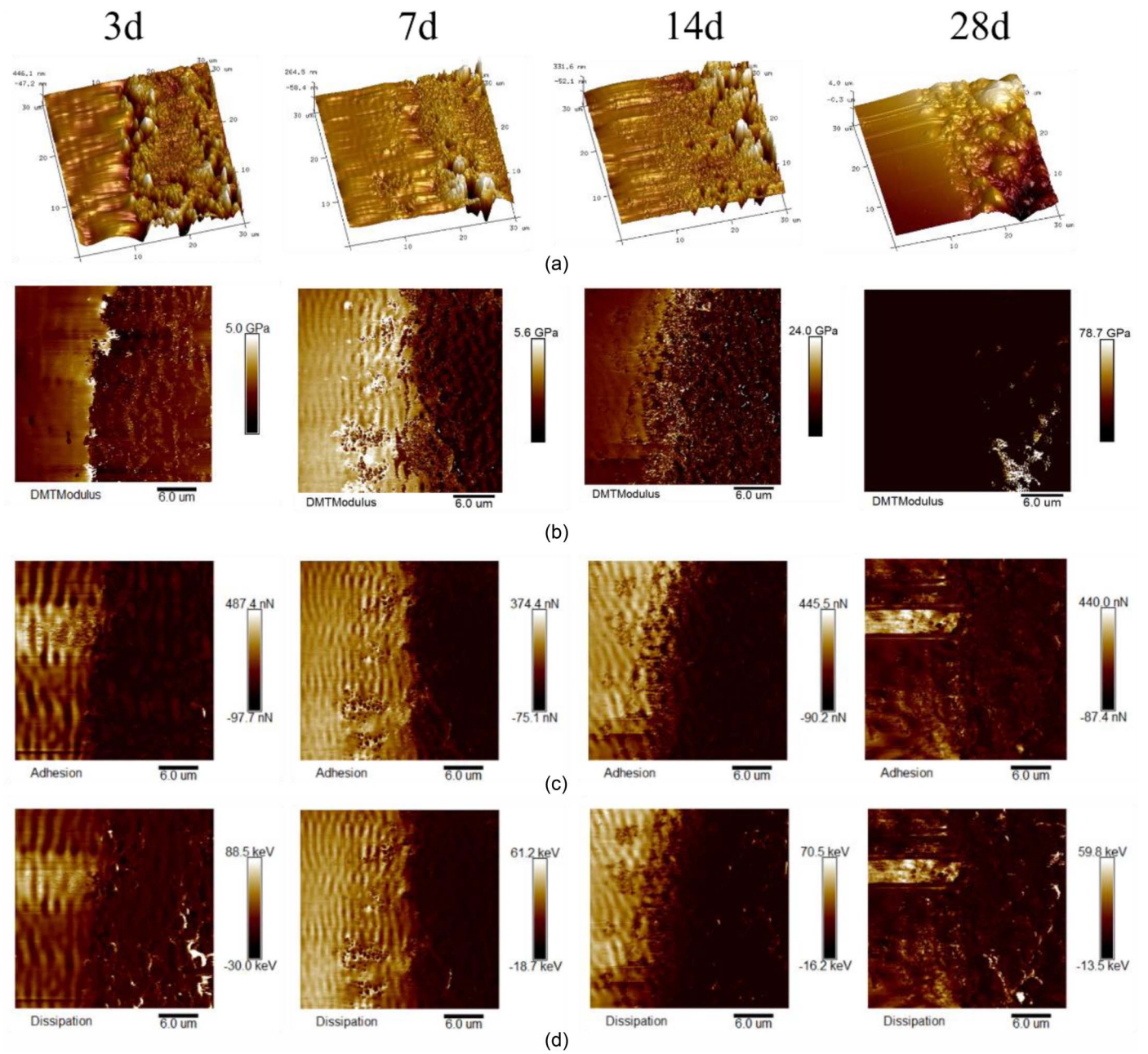

Fig. 6. Microstructural characteristics in GM-60 SFP material with different curing ages using AFM method: (a) Height map; (b) DMT modulus map; (c) Adhesion map; and (d) dissipation map. Note that a smooth surface on the left image indicates asphalt materials while a rough surface on the right indicates cementitious grout materials.

J. Mater. Civ. Eng., 2026, 38(1): 04025479

The asphalt and cementitious grout have a clear sunken boundary at the curing age of 3 d. After the curing age reaches 7 days, the boundary gradually disappears and the ITZ between asphalt and cementitious grout becomes closer. When it reaches 28 days, the sharp microscopic features in the cementitious grout gradually vanish due to asphalt infiltration. The ITZ elevation peak decreases from 446.1 nm to 264.5 nm at 7 days and 331.6 nm at 14 days. By 28 days, the ITZ remains relatively stable, exhibiting minimal fluctuations and an almost flat profile at -1.7 μm. As a result, the interfacial area between asphalt and grout increases greatly and the peak height decreases with increasing curing age.

Comparing the DMT modulus map of the microstructural characteristics of the asphalt–grout interface in the SFP material, as well as their adhesion map and dissipation map at different curing ages using the AFM method in Figs. 6(b–d). It is evident that at curing ages of 3–7 days, relatively distinct boundaries appear at the junction of asphalt and cementitious grout. At a curing age of 14 days, the boundary of the ITZ between asphalt and grout becomes more blurred and dispersed. The findings confirm that the ITZ between asphalt and grout remains active and continues to evolve as the curing process advances in SFP.

To further explore the impact of different curing ages on the ITZ in SFP materials, the DMT modulus distribution of the ITZ in GM-60 SFP materials at different curing ages is illustrated in Fig. 7. Note that the significant drop or changes sharply in vertical coordinates of DMT modulus area correspond to the ITZ area (Chu et al. 2025). In contrast, small vertical coordinate fluctuations and regular fluctuations indicate the asphalt or cementitious grout area (Zhang et al. 2023b). It is evident that as the curing age increases, the ITZ range gradually expands. The asphalt–grout composite ITZ is approximately 5 μm at a curing age of 3 days. At a curing age of 7 days, the ITZ extends to a range of 5–10 μm, and this range continues to increase by the time the curing age reaches 28 days. The reason is that as the curing age increases, interactions between asphalt and cementitious grout at the interface become more intense, allowing substances to spread more widely and gradually expanding the ITZ. Additionally, the continuous formation of hydration products, such as calcium silicate hydrate (C–S–H) and calcium hydroxide [$Ca(OH)_2$], progressively fills the pores in the interface region, contributing to the thickening of the ITZ. In an open environment, $Ca(OH)_2$ in the grout may react with CO_2 in the air, forming calcium carbonate ($CaCO_3$). This carbonation

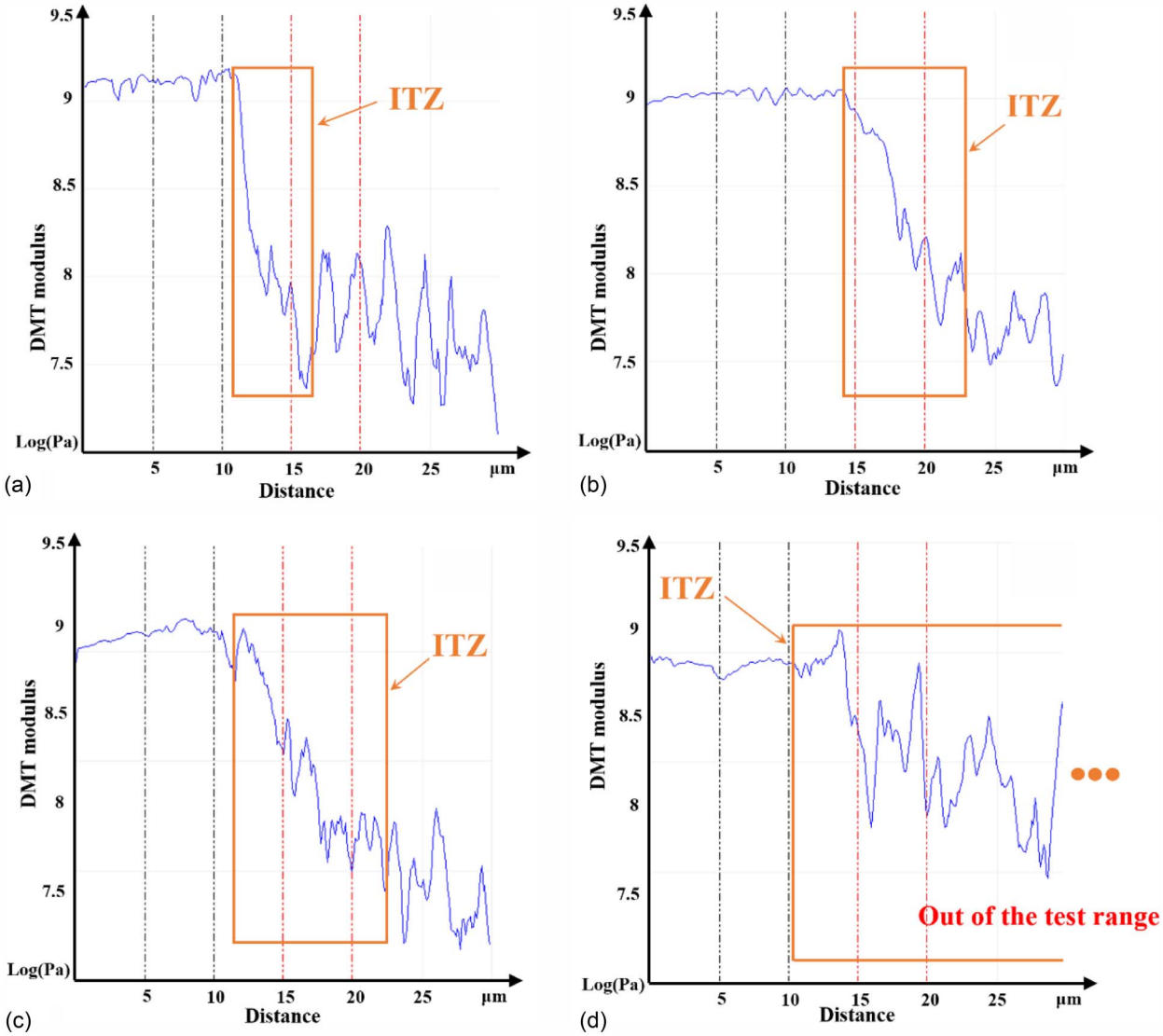

Fig. 7. DMT Modulus distribution in SFP material (GM-60) with a curing age at (a) 3 days; (b) 7 days; (c) 14 days; and (d) 28 days.

J. Mater. Civ. Eng., 2026, 38(1): 04025479

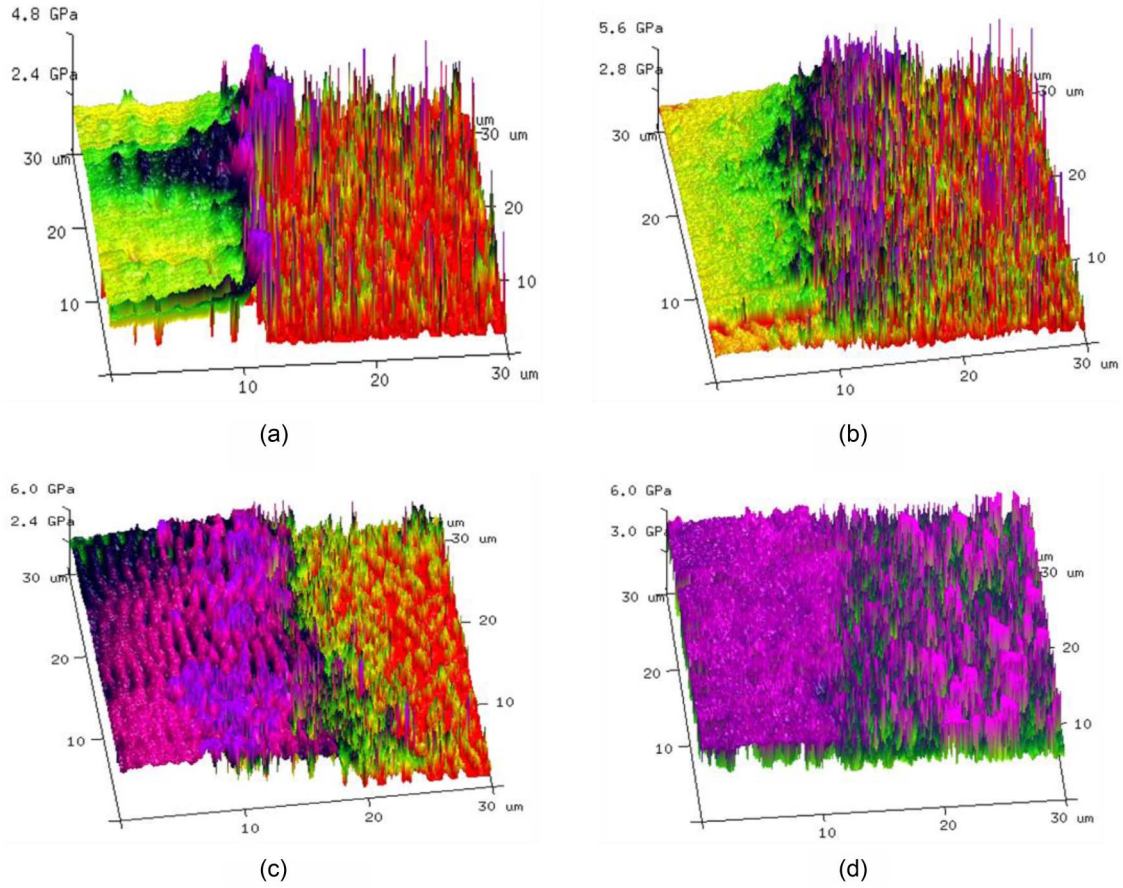

Fig. 8. 3D map of DMT Modulus distribution in SFP material (GM-60) with a curing age at: (a) 3 days; (b) 7 days; (c) 14 days; and (d) 28 days.

process can alter the ITZ microstructure and further increase its thickness. Due to the limited observation area of AFM, it can be inferred that after 28 days, the width of the ITZ between asphalt and grout could exceed 30 μm.

The DMT modulus data of the asphalt–grout ITZ was further analyzed, and the 3D distribution diagram of the DMT modulus in the asphalt–grout ITZ with increasing curing age was obtained, as shown in Fig. 8. The results show that the DMT modulus in each image is roughly divided into four areas. There are two obvious purple and dark blue areas between asphalt and cementitious grout. When the curing age is 3 days, the purple and dark blue areas appear in clear strips. With the age increasing to 7 days, more purple dots appear in the red cementitious grout material area, and the dark blue area blends closely with the purple area. By the 14th day of curing, the originally green asphalt area on the left had penetrated the original red cementitious grout area on the right, and the dark blue and purple areas originally located at the junction had almost completely covered the original green asphalt area on the left. Until the curing age of 28 days, the entire AFM observation area of 30 μm 30 μm $\times$ 30 μm is almost completely covered by purple and dark blue, indicating that asphalt and cementitious grout are on either side of the contact ITZ.

A distinct state or substance, different from that of the body, forms between the asphalt and the grout material, resulting in a DMT modulus that differs from that of the body. As the curing age increases, the interaction between the asphalt and cementitious grout materials intensifies. Consequently, this substance or state gradually expands, leading to an almost uniform DMT modulus throughout the entire observation range. In conclusion, according to the DMT modulus variation trend of the asphalt-cementitious grout ITZ with the curing age, considering that the AFM observation range is limited and the ITZ modulus in a larger range cannot be captured, it can still be found that the modulus regions on both sides of the interface are closer to the modulus of the bulk. Only through the modulus variation trend in the current 30 μm x 30 μm area, it can be demonstrated that there is a double-layer interface structure at the junction of asphalt and cement slurry. One layer is close to the asphalt and the other is close to the cement slurry. The interface structure on both sides is different from the bulk material, which also confirms the theory that there is a double-layer structure at the interface of organic-inorganic composite materials (i.e., The structure of the interface layer of the composite material is composed of the surface layer of the two phases and the region with a certain thickness that penetrates into the two phases due to the interaction between the two phases.).

Interface Impact Analysis

This section further examines the composite interfaces of three cementitious grout materials and asphalt after 28 days of standard curing. AFM observations were also conducted on the interactive interface between three types of cementitious grout materials and asphalt after immersion in the modifier. Fig. 9 shows the AFM height maps of the interface between the asphalt and the three cementitious grout materials before and after interfacial enhancement. It can be seen from Fig. 7 that the height in the left maps is consistently slightly higher than that in the right maps, and there are no obvious continuous depressions and gullies in the right maps. The reason is that the interfacial modifier enhances the interfacial interaction, resulting in more frequent interactions between surface materials and a more uniform surface. Therefore, the asphalt–grout

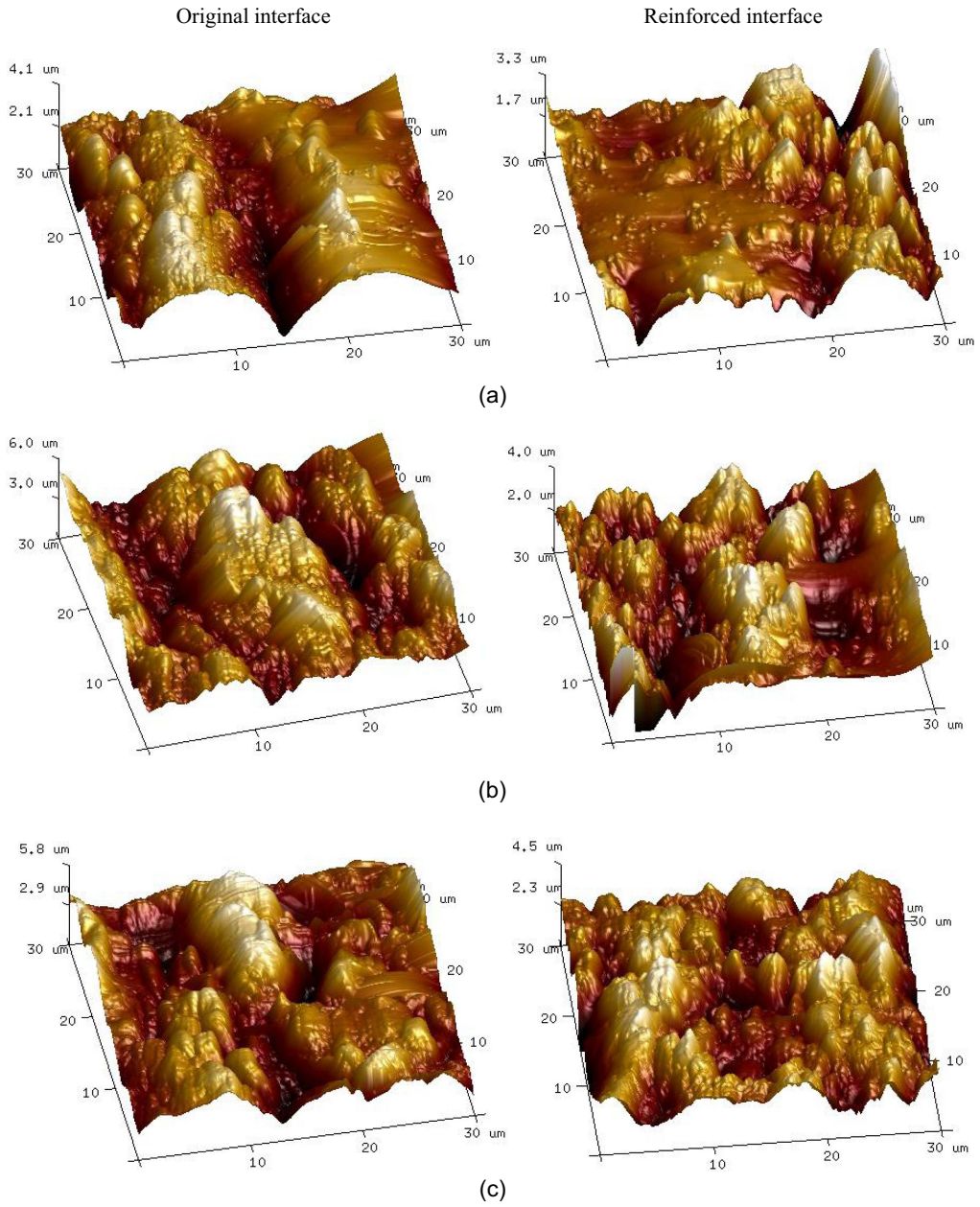

Fig. 9. 3D height map of the original interface and reinforced interface between asphalt: (a) GM-40; (b) GM-60; and (c) GM-70 grout materials.

interface treated with the silane coupling agent solution improves the SFP, resulting in a tighter connection between the organic asphalt concrete skeleton and the inorganic cementitious grout material, as well as a more uniform and smoother bonding surface.

Comparative Study

Fig. 10 shows the DMT modulus maps of the ITZ between asphalt and three grout materials after interface enhancement. It can be seen that the DMT modulus of the interface between the three grout materials and asphalt shows little variation within the 30 μm 30 μm $\times$ 30 μm range. The peak modulus value is generally consistent with the macroscopic compressive strength behavior of the three grout materials (Liu et al. 2023).

It can be also seen in Fig. 10 that the ITZ between the grout materials and asphalt reaches 30 μm due to the effect of the interface modifier because there is little difference in DMT modulus within the 30 μm $\times$ 30 μm range. In addition, the modulus peak within the observation range increased significantly, which was significantly different from the modulus peak of the ordinary interface. The corresponding interface between the grout materials and asphalt was significantly different in structure before and after the interface modifier. The results indicate that immersion of the PAM specimens in a silane coupling agent solution before pouring the cementitious grout material enhances the interface interaction. This leads to a closer observation of the two-phase materials under AFM. Additionally, the overall DMT modulus of the specimens treated with the silane coupling agent is higher than that of the untreated specimens.

The amount of adhesion can reflect the microscopic viscosity of the material. Conventional asphalt pavement materials are prone to water damage due to reduced adhesion. Fig. 11 depicts the adhesion force in the ITZ between asphalt and three types of cementitious grout materials before and after interfacial enhancement. As shown in Fig. 11, the peak points are not clustered but

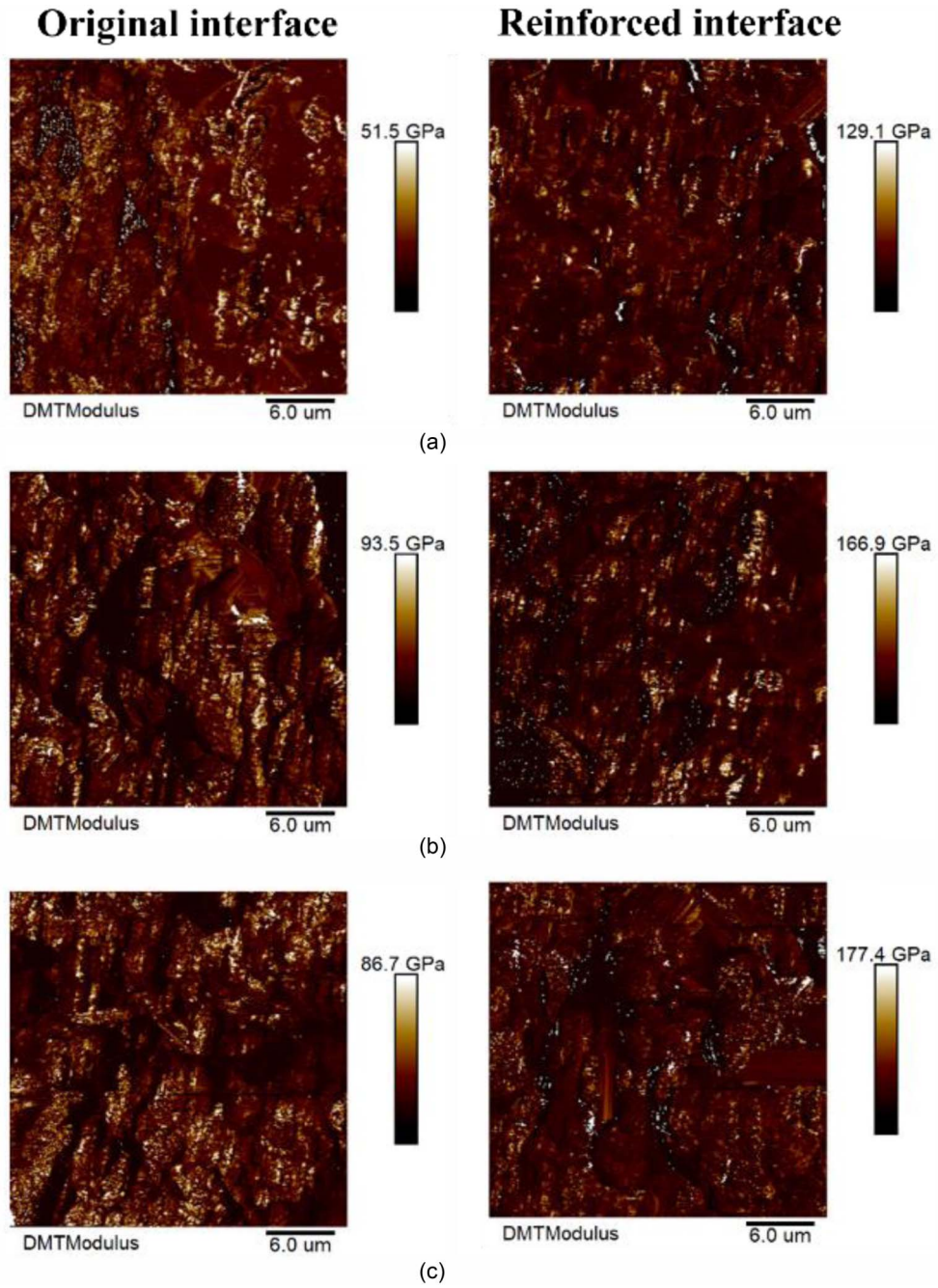

Fig. 10. DMT modulus map of the original interface and reinforced interface between asphalt: (a) GM-40; (b) GM-60; and (c) GM-70 grout materials with a curing age at 28 days.

are more evenly distributed across the entire observation area. For instance, in the original interface, the peaks are concentrated on one side, whereas in the reinforced interface, they are more uniformly spread throughout the figure. Additionally, a noticeable difference in peak distribution can be observed between the original and reinforced interfaces. Therefore, the adhesion force distribution at the asphalt–grout ITZ becomes more pronounced and uniformly larger after enhancement. It reflects that immersion of the asphalt specimen with the interface modifier can enhance the microscopic properties of the ITZ between asphalt and grout. This connection facilitates more uniform microscopic exchange and diffusion of materials.

The dissipated energy ratio is the ratio of dissipated to stored energy, reflecting the material's ability to relax stress. The low-temperature performance of asphalt is directly proportional to dissipated energy and inversely proportional to stored energy. The dissipation energy of the asphalt–grout interfaces before and after enhancement is illustrated in Fig. 12. From these figures, it is evident that the peak values of interfacial dissipation energy between the three cementitious grout materials and asphalt show significant differences before and after reinforcement. The peak value of dissipated energy in the observation area is significantly reduced with the strengthening of the composite interface. This indicates that the enhancement of the composite interface, along with intensive material interaction. In addition, the adhesion of the observed composite interface area to the probe is reduced, and the work required for the probe to contact the observation point and withdraw from the observation point is reduced. This is due to the interaction between the grout and asphalt weakening the adhesion of pure asphalt to the probe.

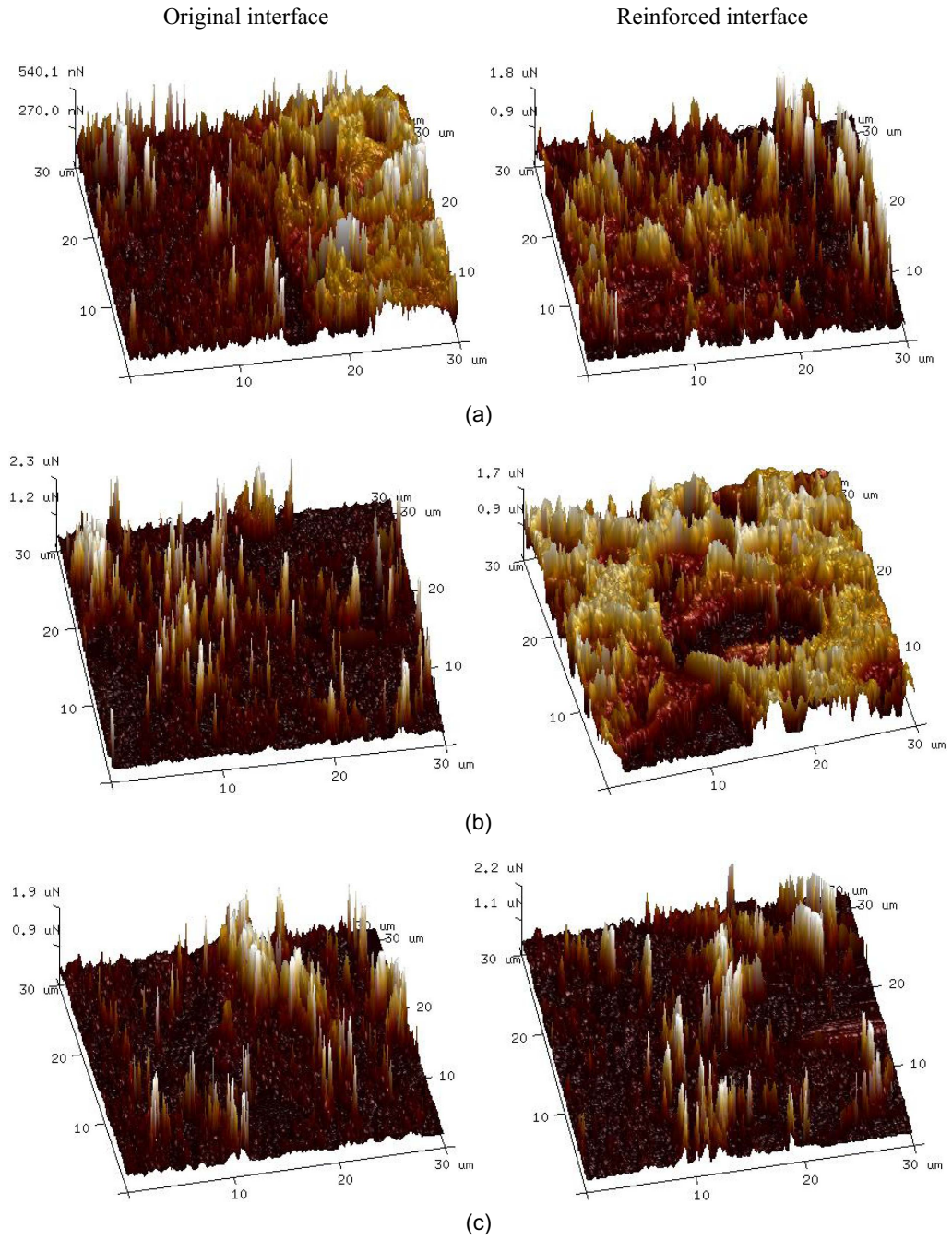

Fig. 11. Adhesion map of the original interface and reinforced interface between asphalt: (a) GM-40; (b) GM-60; and (c) GM-70 grout materials with a curing age at 28 days.

Discussions

Microscopic Morphology Analysis

This section further applied SEM to investigate the microscopic morphology of the asphalt–grout composite interface. Through detailed observation and analysis of the microstructure of the asphalt–grout interface, it reveals its correlation with macroscopic properties. Fig. 13 shows the SEM observation of the ITZ between asphalt and grout before and after using interface modifiers. Note that a higher atomic number means a brighter area in SEM (Cai et al. 2020b). The asphalt, mainly containing C and H, is the darkest area. Before interfacial modification, the ITZ is at the edge of the asphalt phase, and there is an area with obvious variables along the asphalt phase. After the reinforced interface, the elements in the ITZ region interact more densely, and the ITZ region in asphalt and grout cannot be distinguished in the SEM image. The PAM is more closely connected to the three types of cementitious grout materials after immersion in the silane coupling agent. Under the same magnification, obvious cracks are present at the asphalt–grout interface without the use of interface modifiers, and bright band-like areas distinct from the two materials appear on both the asphalt and grout material sides near the interface and the location of this area is along the interface. This area is identified as a weak point in the overall SFP material structure. After the interface enhancement, no microscopic cracks are visible in the transition zone of the asphalt–grout interface. However, there is still a bright band-like area at the interface. This further confirms that the asphalt and cementitious grout materials exhibit a double-layer interface structure, as illustrated in Fig. 14.

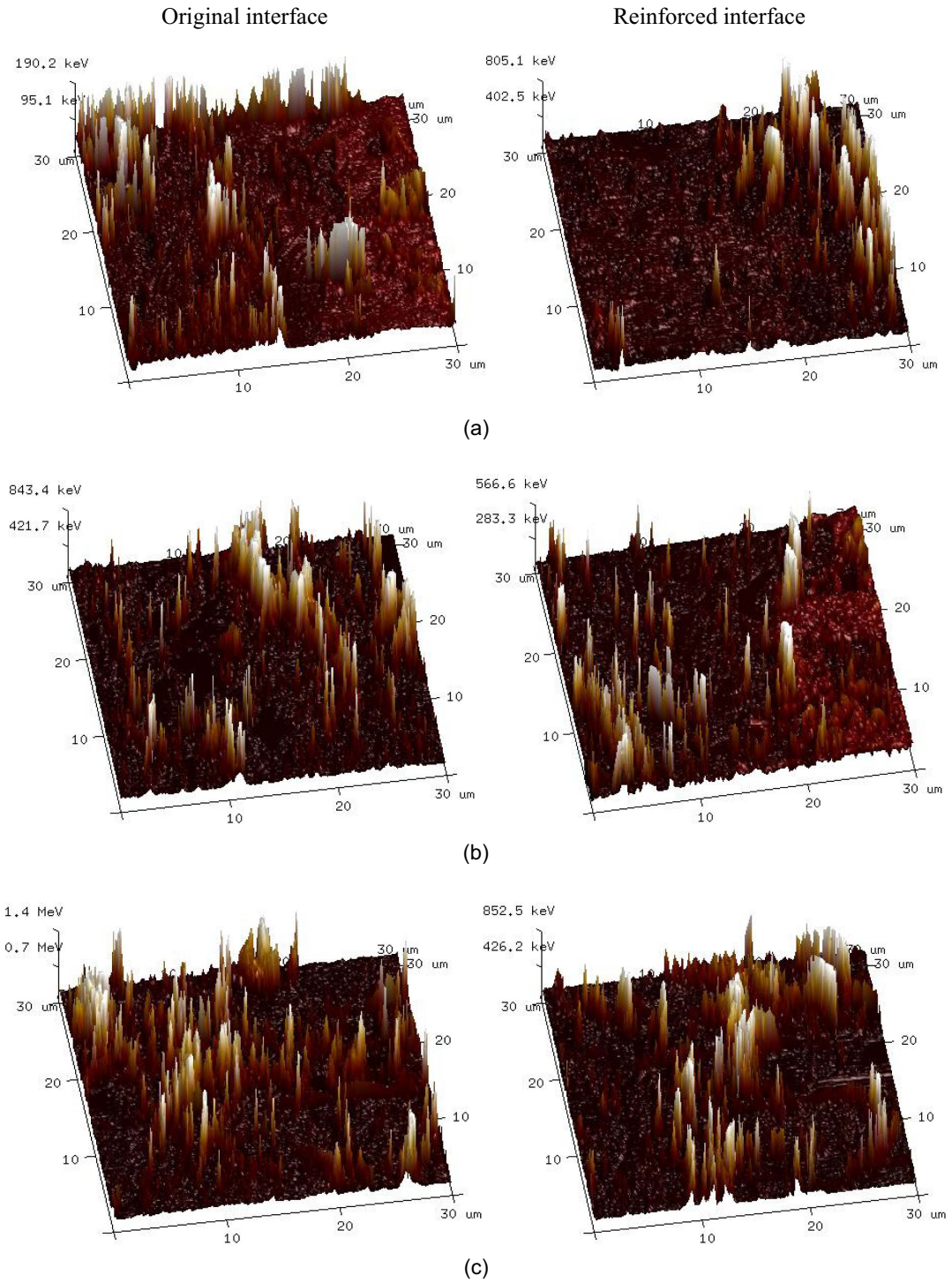

Fig. 12. Dissipation map of the original interface and reinforced interface between asphalt: (a) GM-40; (b) GM-60; and (c) GM-70 grout materials with a curing age at 28 days.

On the other hand, interface structures distinct from the main body exist on both the asphalt side and the cementitious grout material side, further confirming the double-layer theory of the organic-inorganic composite interface. This conclusion aligns with the results of Cai et al. (2020b), which indicate that at least four phases exist at the SFP interface. It means that immersion PAM with a silane coupling agent tightens the asphalt–grout ITZ, indicating that interface modification can reduce delamination at this interface, merging the originally layered ITZ along the material's distribution direction. This enhancement is linked to improved macromechanical properties resulting from changes in the microscopic morphology of the asphalt–grout ITZ after immersion.

Macroscopic Performance Analysis

Through the semicircular bending test, the peak load, peak displacement, fracture energy (G_f), and crack resistance index (CRI) of semiflexible pavement materials can be obtained (Song et al. 2024), with the average value of four specimens taken as the final test result. Note that a high G_f value or a low CRI value means

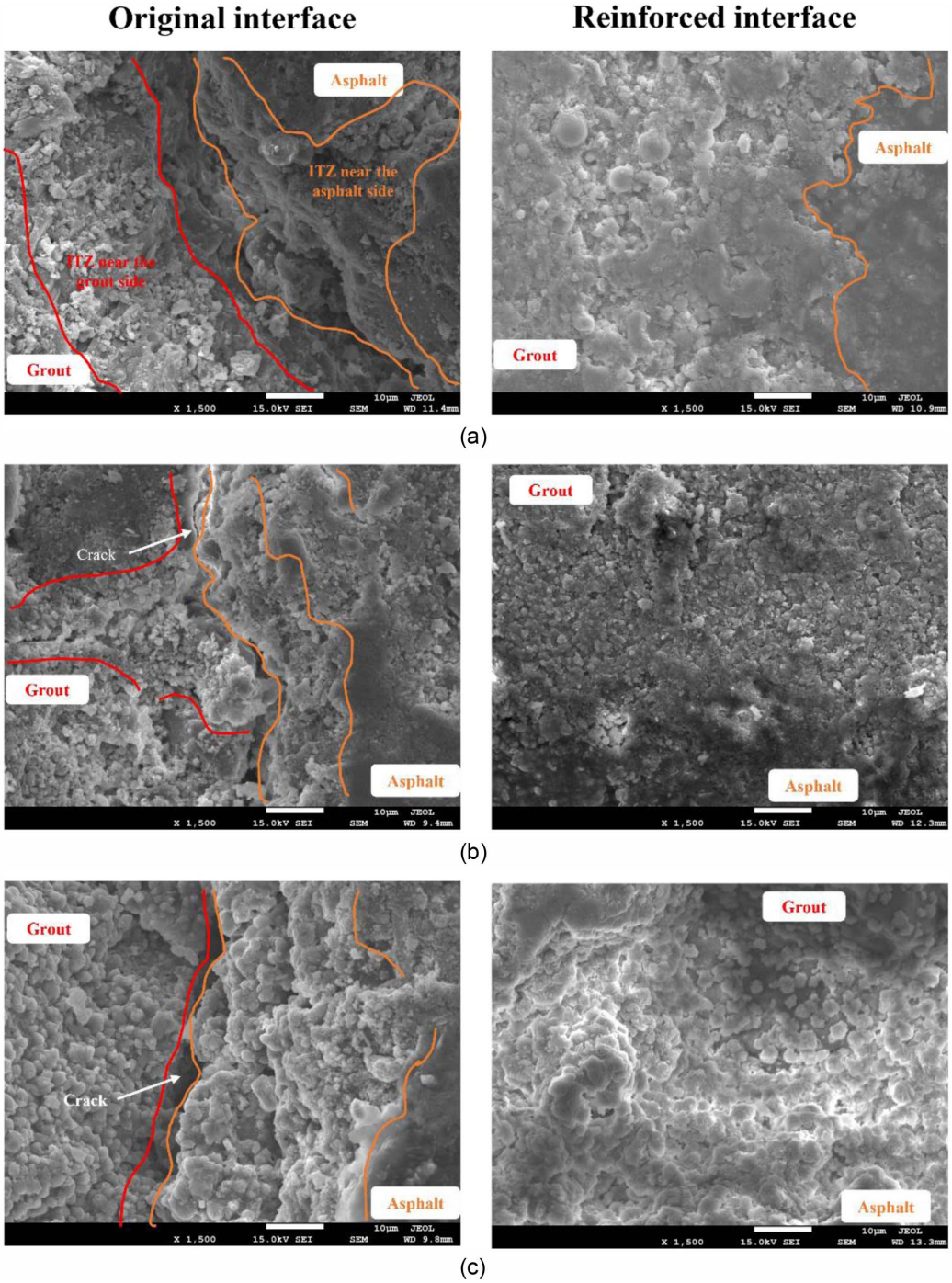

Fig. 13. SEM images of the original interface and the reinforced interface between asphalt: (a) GM-40; (b) GM-60; and (c) GM-70 grout materials with acuring age at 28 days (×1,500).

excellent cracking performance. The results of the semicircular bending test are shown in Table 4. The results in Table 4 demonstrate that the cracking resistance of SFP specimens improved after interface modification. This enhancement is primarily due to the improved adhesive properties of the asphalt, which increase cohesion and strengthen intermolecular interactions. At the microscopic level, interface modification contributes to a more compact and uniform interfacial structure, effectively reducing defects within the asphalt–grout ITZ. This refined microstructure translates into superior mechanical performance on the macroscopic scale. Consequently, immersing SFP specimens in a silane coupling agent solution significantly enhances interfacial strength, ultimately improving the overall material performance.

Conclusions

This paper aims to examine the microstructural interface properties of asphalt–grout ITZ in SFP material after an interfacial modifier using a series of micromechanics techniques. The AFM characterized the asphalt–grout composite ITZ by considering variables such as curing ages, grout strengths, and interface modification status. Additionally, SEM tests were used to explore the correlation between the microscopic morphology and macroscale mechanical

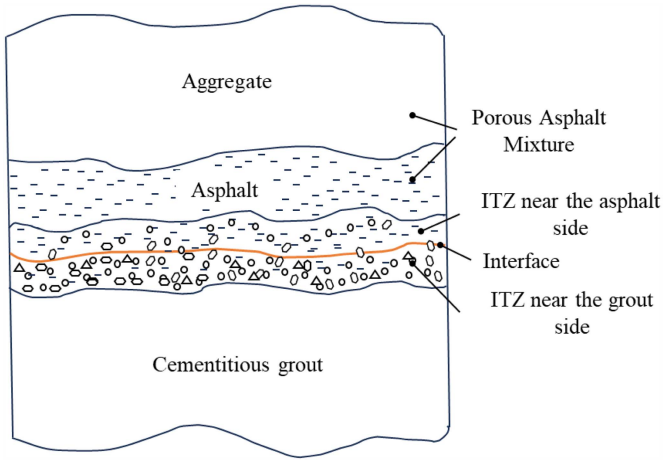

Fig. 14. Illustration of the double-layer interface transition zone in the microstructure of SFP materials.

Table 4. Results of semicircular bending test for SFP formed with GM-40 grouting materials

Interface type	Peak load (kN)	Peak displacement (mm)	G_f (J/m^2)	CRI (J/(N·m^2))
Original interface	1.62	1.3	489.05	301.88
Reinforced interface	3.47	2.1	699.34	201.54

characteristics of the ITZ between asphalt and grout. The following conclusions were drawn from the analyses:

1. ITZ between asphalt and grout persists and continues to interact as the curing age progresses in SFP. The ITZ between asphalt and grout is a double-layer interface structure. The width of the asphalt–grout ITZ may exceed 30 μm after 28 days.
2. ITZ between asphalt and grout immersed with the silane coupling agent solution enhances the formed SFP, resulting in a tighter connection between the organic asphalt concrete skeleton and the inorganic cementitious grout material, as well as a more uniform and smoother bonding surface.
3. Immersion of the PAM specimens with the interface modifier can enhance the microscopic properties of the asphalt and cementitious grout materials. The connection makes the material exchange and diffusion more uniform microscopically.
4. Microcracks in the asphalt–grout ITZ were significantly reduced after interface enhancement, whereas prominent cracks were observed at the asphalt–grout interface when no interfacial modifiers were applied. This area is identified as a weak point in the overall SFP material structure.

The research results elucidate how the composite interface influences the microstructural interface properties of asphalt–grout ITZ, providing theoretical support for the performance optimization of SFP materials. Future work will investigate the chemical composition of SFP with enhanced interfaces and further examine the factors influencing the road performance of SFP materials.

Data Availability Statement

All data, models, and code generated or used during the study appear in the published article.

Acknowledgments

The work described in this paper is supported by the National Natural Science Foundation of China (Nos. 52338005 and 51878193).

Author Contributions

Xiaoyu Liu: Methodology; Software; Visualization; Writing – original draft. Kuanghuai Wu: Funding acquisition; Supervision. Yi Li: Investigation; Project administration. Giovanni Giacomello: Data curation; Writing – review and editing. Yunpeng Yue: Formal analysis; Investigation; Writing – review and editing. Fengming Ren: Conceptualization; Funding acquisition; Investigation. Marco Pasetto: Supervision; Writing – review and editing.

References

AASHTO. 2016. *Standard method of test for determining the fracture potential of asphalt mixtures using semicircular bend geometry (SCB) at intermediate temperature*. AASHTO TP 124-16. Washington, DC: AASHTO.

Abdessalem, A., S. Tamboura, J. Fitoussi, H. B. Daly, A. Tcharkhtchi, and F. Meraghni. 2021. "Microstructure investigation of hydrothermal damage of aged SMC composites using micro-computed tomography and scanning electron microscopy." *Eng. Fail. Anal.* 121 (Mar): 105177. https://doi.org/10.1016/j.engfailanal.2020.105177.

Allen, R. G., N. Little Dallas, and A. Bhasin. 2012. "Structural characterization of micromechanical properties in asphalt using atomic force microscopy." *J. Mater. Civ. Eng.* 24 (10): 1317–1327. https://doi.org/10.1061/(ASCE)MT.1943-5533.0000510.

Cai, X., C. Shi, X. Chen, and J. Yang. 2021. "Identification of damage mechanisms during splitting test on SFP at different temperatures based on acoustic emission." *Constr. Build. Mater.* 270 (Feb): 121391. https://doi.org/10.1016/j.conbuildmat.2020.121391.

Cai, X., J. Yang, X. Chen, J. Zhang, and H. Zhang. 2020a. "Interlocking property evaluation of dual skeleton in semiflexible pavement material by micromechanical model and X-ray computed tomography." *Constr. Build. Mater.* 254 (Sep): 118934. https://doi.org/10.1016/j.conbuildmat.2020.118934.

Cai, X., H. Zhang, J. Zhang, X. Chen, J. Yang, and J. Hong. 2019. "Investigation on reinforcing mechanisms of semiflexible pavement material through micromechanical model." *Constr. Build. Mater.* 198 (Feb): 732–741. https://doi.org/10.1016/j.conbuildmat.2018.11.243.

Cai, X., J. Zhang, H. Zhang, Z. Yao, X. Chen, and J. Yang. 2020b. "Identification of microstructural characteristics in semiflexible pavement material using micromechanics and nano-techniques." *Constr. Build. Mater.* 246 (Jun): 11846. https://doi.org/10.1016/j.conbuildmat.2020.118426.

Cheng, P., G. Ma, and Y. Li. 2023. "Preparation and performance improvement mechanism investigation of high-performance cementitious grout material for semiflexible pavement." *Polymers* 15 (12): 2631. https://doi.org/10.3390/polym15122631.

Chinese Standard. 2011. *Standard test methods of bitumen and bituminous mixtures for highway engineering*. JTG E20-2011. Beijing: Chinese Standard.

Chu, Z., N. Guo, Z. Wang, S. Wang, Z. You, X. Liu, and E. Wu. 2025. "Identification and mechanical properties of asphalt mastic-aggregate interface transition zone (ITZ) based on nanoindentation and AFM." *Constr. Build. Mater.* 461 (Jan): 139898. https://doi.org/10.1016/j.conbuildmat.2025.139898.

Cui, B., X. Gu, H. Wang, and D. Hu. 2021. "Numerical and experimental evaluation of adhesion properties of asphalt-aggregate interfaces using molecular dynamics simulation and atomic force microscopy." *Road Mater. Pavement Des.* 23 (7): 1564–1584. https://doi.org/10.1080/14680629.2021.1910547.

Davoodi, A., M. Aboutalebi Esfahani, M. Bayat, S. E. Mohammadyan-Yasouj, and A. Rahman. 2022. "Influence of nano-silica modified rubber mortar and EVA modified porous asphalt on the performance improvement of modified semiflexible pavement." *Constr. Build. Mater.* 337 (Jun): 127573. https://doi.org/10.1016/j.conbuildmat.2022.127573.

Fan, J., M. Gong, L. Jiang, J. Cheng, S. Li, Z. Li, X. Zhu, and J. Hong. 2024. "Interlayer failure characteristics of semiflexible composite pavement structures (SFCPS) at high temperatures." *Constr. Build. Mater.* 441 (Aug): 137563. https://doi.org/10.1016/j.conbuildmat.2024.137563.

Fan, S., C. Gao, G. Yang, Y. Zhang, C. Zhang, N. Song, S. Zhang, P. Zhang, Z. Zhang, and S. Ke. 2021. "Enhancing wear-resistance of Cu nanowires filled polyetheretherketone-based composites under water lubrication conditions via magnetic response to tribofilm." *Tribol. Int.* 153 (Jan): 106601. https://doi.org/10.1016/j.triboint.2020.106601.

Gao, M., H. Zhang, H. Yang, Y. Li, L. Yu, and S. Zhao. 2023. "Research on surface morphology characteristics and micro-damage mechanism of asphalt mastic based on charge transfer principle." *Constr. Build. Mater.* 391 (Aug): 131686. https://doi.org/10.1016/j.conbuildmat.2023.131686.

Gao, Y., X. Zhu, D. J. Corr, M. S. Konsta-Gdoutos, and S. P. Shah. 2019. "Characterization of the interfacial transition zone of CNF-Reinforced cementitious composites." *Cem. Concr. Compos.* 99 (May): 130–139. https://doi.org/10.1016/j.cemconcomp.2019.03.002.

Guo, F., J. Pei, J. Zhang, B. Xue, G. Sun, and R. Li. 2020. "Study on the adhesion property between asphalt binder and aggregate: A state-of-the-art review." *Constr. Build. Mater.* 256 (Sep): 119474. https://doi.org/10.1016/j.conbuildmat.2020.119474.

Hoy, M., S. Horpibulsuk, A. Arulrajah, and A. Mohajerani. 2018. "Strength and microstructural study of recycled asphalt pavement: Slag geopolymer as a pavement base material." *J. Mater. Civ. Eng.* 30 (8): 04018177. https://doi.org/10.1061/(ASCE)MT.1943-5533.0002393.

Hu, C., Z. Zhou, and Y. Luo. 2023. "Study on damage evolution and mechanism of semiflexible pavement under acid rain erosion." *Case Stud. Constr. Mater.* 19 (Dec): e02286. https://doi.org/10.1016/j.cscm.2023.e02286.

Kandhal, P. S., and S. Chakraborty. 1996. "Effect of asphalt film thickness on short-and long-term aging of asphalt paving mixtures." *Transp. Res. Rec.* 1535 (1): 83–90. https://doi.org/10.1177/0361198196153500111.

Lai, T., R. Wang, and T. Zhu. 2024. "Evolution behavior of adhesion force with continually changed relative humidity revealed on AFM." *J. Adhes.* 100 (16): 1623–1660. https://doi.org/10.1080/00218464.2024.2343409.

Lin, M., J. Shuai, P. Li, X. Kang, and Y. Lei. 2022. "Analysis of rheological properties and micro-mechanism of aged and reclaimed asphalt based on multi-scales." *Constr. Build. Mater.* 321 (Feb): 126290. https://doi.org/10.1016/j.conbuildmat.2021.126290.

Ling, S., Z. Chen, D. Sun, H. Ni, Y. Deng, and Y. Sun. 2022a. "Optimal design of pouring semiflexible pavement via laboratory test, numerical research, and field validation." *Transp. Res. Rec.* 2676 (11): 479–495. https://doi.org/10.1177/03611981221093631.

Ling, S., P. Igor Itoua, D. Sun, and D. Jelagin. 2022b. "Damage characterization of pouring semiflexible pavement material under triaxial compressive load based on X-ray computed tomography." *Constr. Build. Mater.* 348 (Sep): 128653. https://doi.org/10.1016/j.conbuildmat.2022.128653.

Ling, S., F. Yu, D. Sun, G. Sun, and L. Xu. 2021. "A comprehensive review of tire-pavement noise: Generation mechanism, measurement methods, and quiet asphalt pavement." *J. Cleaner Prod.* 287 (Mar): 125056. https://doi.org/10.1016/j.jclepro.2020.125056.

Liu, X., K. Wu, X. Cai, W. Huang, and J. Huang. 2023. "Influence of the composite interface on the mechanical properties of semiflexible pavement materials." *Constr. Build. Mater.* 397 (Mar): 132466. https://doi.org/10.1016/j.conbuildmat.2023.132466.

Liu, X., K. Wu, G. Giacomello, X. Cai, and M. Pasetto. 2025a. "Numerical analysis of mechanical properties at the internal interface of SFP material using a digital image algorithm." *Mater. Struct.* 58 (1): 43. https://doi.org/10.1617/s11527-025-02575-3.

Liu, X., K. Wu, G. Giacomello, Y. Yue, F. Ren, X. Cai, and M. Pasetto. 2025b. "Enhancing cracking resistance in semiflexible pavements using an interfacial immersion method." *Case Stud. Constr. Mater.* 22 (Jul): e04311. https://doi.org/10.1016/j.cscm.2025.e04311.

Pei, J., J. Cai, D. Zou, J. Zhang, R. Li, X. Chen, and L. Jin. 2016. "Design and performance validation of high-performance cement paste as a grouting material for semiflexible pavement." *Constr. Build. Mater.* 126 (Nov): 206–217. https://doi.org/10.1016/j.conbuildmat.2016.09.036.

Pouliot, N., J. Marchand, and M. Pigeon. 2003. "Hydration mechanisms, microstructure, and mechanical properties of mortars prepared with mixed binder cement slurry-asphalt emulsion." *J. Mater. Civ. Eng.* 15 (1): 54–59. https://doi.org/10.1061/(ASCE)0899-1561(2003)15:1(54).

Qiang, W., Y. Peiyu, A. Ruhan, Y. Jinbo, and K. Xiangming. 2011. "Strength mechanism of cement-asphalt mortar." *J. Mater. Civ. Eng.* 23 (9): 1353–1359. https://doi.org/10.1061/(ASCE)MT.1943-5533.0000301.

Raza, M. S., and S. K. Sharma. 2024. "A review of mechanical and durability properties and microstructure of semiflexible pavement." *Innovative Infrastruct. Solutions* 9 (4): 83. https://doi.org/10.1007/s41062-024-01393-w.

Ren, M., T. Shi, D. J. Corr, and S. P. Shah. 2019. "Mechanical properties of micro-regions in cement-based material based on the PeakForce QNM mode of AFM." *J. Wuhan Univ. Technol. Mater. Sci. Ed.* 34 (Aug): 893–899. https://doi.org/10.1007/s11595-019-2134-7.

Song, J., B. Chen, M. Sun, K. Wu, J. Chen, and X. Cai. 2024. "Study on the improvement of fatigue and crack resistance of semiflexible pavement materials using the mixing-molding method." *Constr. Build. Mater.* 450 (Nov): 138728. https://doi.org/10.1016/j.conbuildmat.2024.138728.

Sui, X., Z. Leng, S. Wang, X. Cai, M. Gong, and L. Zhang. 2024. "In-situ grouting rate prediction of semiflexible pavement based on a novel composite dielectric constant model and ground-penetrating radar." *Constr. Build. Mater.* 438 (Aug): 137209. https://doi.org/10.1016/j.conbuildmat.2024.137209.

Wang, S., H. Zhou, X. Chen, M. Gong, J. Hong, and X. Shi. 2021. "Fatigue resistance and cracking mechanism of semiflexible pavement mixture." *Materials* 14 (18): 5277. https://doi.org/10.3390/ma15010014.

Wu, K., X. Liu, X. Cai, W. Huang, J. Yu, and G. Nie. 2021. "Performance and fracture analysis of composite interfaces for semiflexible pavement." *Coatings* 11 (10): 1231. https://doi.org/10.3390/coatings11101231.

Xie, H., Y. Liu, Z. Long, F. Xu, L. You, X. Tang, C. Zhu, and Y. Ding. 2023. "Micro-characterization of the adhesion properties and mechanisms at the asphalt-silica aggregate interface under combined thermal-oxygen aging and chloride salt erosion." *Constr. Build. Mater.* 401 (Oct): 132818. https://doi.org/10.1016/j.conbuildmat.2023.132818.

Xu, W., X. Qiu, S. Xiao, G. Hu, F. Wang, and J. Yuan. 2020. "Molecular dynamic investigations on the adhesion behaviors of asphalt mastic—Aggregate interface." *Materials* 13 (22): 5061. https://doi.org/10.3390/ma13225061.

Xu, Z., Z. Bai, J. Wu, H. Long, H. Deng, Z. Chen, Y. Yuan, and X. Fan. 2022. "Microstructural characteristics and nano-modification of interfacial transition zone in concrete: A review." *Nanotechnol. Rev.* 11 (1): 2078–2100. https://doi.org/10.1515/ntrev-2022-0125.

Zarei, S., J. Ouyang, and Y. Zhao. 2022. "Evaluation of fatigue life of semiflexible pavement with cement asphalt emulsion pastes." *Constr. Build. Mater.* 349 (Sep): 128797. https://doi.org/10.1016/j.conbuildmat.2022.128797.

Zhang, K., S. Guan, X. Liu, C. Yao, L. Yan, and W. Fan. 2023a. "Macro- and micro-mechanical properties of flawed sandstone and their degradation mechanisms under hydrodynamic scouring." *Eng. Fract. Mech.* 292 (Nov): 109665. https://doi.org/10.1016/j.engfracmech.2023.109665.

Zhang, L., S. Zhou, Z. Xiong, Z. Mo, Q. Lu, and J. Hong. 2024a. "Research on the crack resistance of semiflexible pavement mixture based on meso-heterogeneous model." *Constr. Build. Mater.* 411 (Jan): 134495. https://doi.org/10.1016/j.conbuildmat.2023.134495.

Zhang, M., C. Kou, A. Kang, P. Xiao, and H. Hu. 2023b. "Microscopic characteristics of interface transition zones of hot mix asphalt containing recycled concrete aggregates." *J. Cleaner Prod.* 389 (Feb): 136070. https://doi.org/10.1016/j.jclepro.2023.136070.

Zhang, M., Z. Xiong, M. Gong, J. Hong, H. Qiao, Y. Zhang, and L. Jiang. 2024b. "Multi-scale damage characterisation of semiflexible pavements under freeze-thaw cycles." *Constr. Build. Mater.* 445 (Sep): 137847. https://doi.org/10.1016/j.conbuildmat.2024.137847.

Zhang, Y., K. Yao, Z. Yi, Z. Li, H. Li, W. Zang, and Y. Zhang. 2024c. "Evaluation for water stability of bitumen mixture with multi-scale method." *Constr. Build. Mater.* 412 (Jan): 134836. https://doi.org/10.1016/j.conbuildmat.2023.134836.

Zhao, D., X. Ma, H. Wang, and C. Zhang. 2023. "Investigation of the wet and thermal conditions effect on the micro-scale characteristics of interfacial transition zone of porous asphalt mixture." *Coatings* 13 (3): 566. https://doi.org/10.3390/coatings13030566.

Zhao, W., and Q. Yang. 2022. "Study on the applicability of asphalt concrete skeleton in the semiflexible pavement." *Constr. Build. Mater.* 327 (Apr): 126923. https://doi.org/10.1016/j.conbuildmat.2022.126923.

Zhu, X., Y. Yuan, L. Li, Y. Du, and F. Li. 2017. "Identification of interfacial transition zone in asphalt concrete based on nano-scale metrology techniques." *Mater. Des.* 129 (Sep): 91–102. https://doi.org/10.1016/j.matdes.2017.05.015.